

Towards Automated Ear Surgery: Improved Calibration and Registration Procedures



WPI

Submitted by:

Shannon L. Harrington
Christopher A. Salomone

Submitted to:

Marko Popovic Ph.D., Advisor, WPI
Cosme Furlong-Vazquez Ph.D., Co-Advisor, WPI
Ivo Dobrev Ph.D., Co-Advisor, UniversitätsSpital Zürich

October 12, 2017

A Major Qualifying Project Report: submitted to the Faculty of: WORCESTER POLYTECHNIC INSTITUTE in partial fulfillment of the requirements for: Degree of Bachelor of Science.

Abstract

A micro-electro-mechanical system (MEMS) based hydrophone inserted into the cochlea may be utilized to study acoustic pressure distribution. The objective of this project, performed through collaboration between WPI and UniversitätsSpital Zürich, was to develop an improved procedure for experiments at the UniversitätsSpital Zürich that would increase the insertion accuracy. This is necessary due to the small scale, complex anatomy, and delicate nature of the inner ear. This was done by calibrating tools and completing registration and insertion processes. The goal was to achieve an overall accuracy of 250 microns, which was met with a final accuracy below 200 microns, suggestive that the devised procedure can provide an accurate roadmap for future experiments.

Acknowledgments

We would first like to thank our host at the UniversitätsSpital Zürich, Dr. Ivo Dobrev, for his extraordinary dedication to this project and the countless hours he spent helping us. We would also like to thank the other members of the team at the UniversitätsSpital Zürich, including Lukas Prochazka, Flurin Pfiffner, and Jae Hoon Sim for their help on our project and in making our time in Switzerland enjoyable. We also want to thank our advisor, Professor Marko Popovic, for his useful insight into our project and our co-advisor Professor Cosme Furlong.

Table of Contents

Abstract.....	2
Acknowledgments.....	3
Table of Contents.....	4
List of Figures.....	5
List of Tables.....	5
Chapter 1: Introduction.....	6
Chapter 2: Background.....	7
Anatomy of the Human Ear.....	7
Middle and Inner Ear Research.....	8
<i>Extent of Current Research</i>	8
<i>Research at the UniversitätsSpital Zürich (USZ)</i>	9
Minimally Invasive Surgical Techniques.....	11
CT Scanning.....	12
Errors Within Image Registration Systems.....	12
Chapter 3: Objectives.....	12
Chapter 4: Methodology.....	13
Initial Registration.....	16
Virtual Registration.....	17
Point to Point Cloud Registration.....	17
Final Procedure Test.....	18
Chapter 5: Experimentation and Results.....	20
Initial Registration.....	20
<i>Fiducial Localization Error</i>	20
Final Procedure.....	22
<i>Fiducial Registration Error Using Force Sensor</i>	22
<i>Target Registration Error Based on Six Hydrophone Insertions at two Angles</i>	23
Chapter 6: Discussion.....	24
References.....	27
Appendix A: Current Pressure Experiment Procedure.....	29
Appendix B: Physical and Virtual Registration Data for Initial Registration.....	30
Appendix C: Physical and Virtual Registration Data for Final Procedure.....	32
Appendix D: Point to Point Cloud Registration Parameters.....	33
Appendix E: Preoperative Planning Data for Marker Insertions.....	37

List of Figures

Figure 1 - Diagram of the Ear, (Ear Anatomy, 2006).....	7
Figure 2 - Cross Section View of Cochlea (Sim, 2016)	8
Figure 3 - Ear anatomy with the hydrophone inserted into the cochlea (Pfiffner et al., 2016)	9
Figure 4 - Representation of future pressure experiments with multiple hydrophone insertions.	10
Figure 5 - CAD Model of Hydrophone (Pfiffner et al., 2016).....	10
Figure 6 - Close up of Hydrophone Tip (Left) Hydrophone Tip Dimensions (Right)	11
Figure 7 - Overview of Improved Pressure Experiment Procedure.....	14
Figure 8 - Tool Calibration Setup	15
Figure 9 - Overlay Showing Tool Movement with Measurement Lines	15
Figure 10 - Physical Registration Setup.....	16
Figure 11 - Virtual Reconstruction of Temporal Bone Sample	17
Figure 12 - Post Operative CT Scan Reconstruction	20
Figure 13 - FLE for AMIRA.....	21
Figure 14 - FLE for the Force Sensor	21
Figure 15 - FLE for the Metal Stylus.....	22
Figure 16 - Overview of all FRE per combination, per marker and per point-cloud average for Angle 1	22
Figure 17 - Overview of all FRE per combination, per marker and per point-cloud average for Angle 2	23

List of Tables

Table 1 - Target Registration Error for Six Insertions.....	24
---	----

Chapter 1: Introduction

Currently, a research team at UniversitätsSpital Zürich (USZ) is investigating the acoustic pressure distribution within the inner ear, specifically within the cochlea. They require a method of accessing inside the scala tympani and scala vestibuli of the cochlea by drilling the surrounding temporal bone in order to insert a micro-electro-mechanical system (MEMS) based hydrophone (Pffiffner et al., 2016). They have been unable to carry out this drilling and insertion process in a reliable manner and with suitable accuracy for their experiments.

The main problem stems from switching tools during this process. In total, there are three tools involved across all steps of the full procedure: a metal stylus, an otology drill, and a hydrophone. The metal stylus is used to physically touch the sample during the registration process and then is switched out with either the drill or the hydrophone. Due to the unique geometrical characteristics of each tool they are unable to switch between them while remaining at the same target location. The tip location of each tool is different, with significant enough deviation to cause potential problems of damaging the cochlea or the hydrophone during the drilling and insertion processes. In addition, the exact location (within 100-200 microns) of the measurement position of the hydrophone is determined only after the experiment, thus allowing for uncertainty in the results and their interpretation. Currently, there are no commercially available and/or cost-effective medical systems that allow for the location or calibration of the tools relative to the samples of interest, with a sufficient level of accuracy of 250 microns.

The overall goal of this project was to improve the current drilling and insertion procedure used for the pressure research. The intentions were to develop a procedure that is more repeatable while also providing options for guided or semi-automated drilling and insertion techniques. In order to complete this requirement, one of the main tasks was to create a tool calibration setup and procedure in which the metal stylus, drill, and hydrophone were all calibrated so that their tips are at the same location relative to the manipulator wrist. This allows for the use of a preoperatively calculated approach trajectory and would identify the final location of each tool throughout the entire process to reduce the uncertainty of the measurement results. The objective was to improve the current procedure to have an accuracy of 250 microns during the insertion of these hydrophones. This procedure could then be used for several future applications, such as autonomous or semi-autonomous drilling. Insertions at multiple different locations along the length of the cochlea could also be achieved with this location accuracy.

Chapter 2: Background

Anatomy of the Human Ear

In order to fully understand the nature of this research, it is necessary to first have an understanding of the human ear anatomy. According to Sim (2016), ears are generally broken down into three separate sections: the outer, middle, and inner ear as shown in Figure 1. The outer ear, which is the external part of the ear, consists of the pinna and the ear canal. The main roles of the outer ear are gathering sound and providing a pathway of the sound to the eardrum (also called tympanic membrane). The middle ear consists of the tympanic membrane (TM) and the middle ear ossicular chain suspended inside of the middle ear cavity. The main role of the middle ear is converting sound waves in air to the vibration of cochlear fluid. Sound waves in the ear canal vibrate the TM, and the motion of TM is transmitted to the cochlea via the middle ear ossicular chain. At the oval window, where the stapes interfaces with cochlear fluid, the vibrational motion of the middle ear ossicular chain is converted into fluid vibration. The inner ear, which is where the main focus of this research lies, consists of the cochlea and three semicircular ducts. While the semicircular ducts work for balancing, the cochlea performs the conversion of fluid fluctuation to electrochemical impulses, which are delivered to the brain via auditory nerves. It is within the cochlea that the transition from the mechanical systems to the electrochemical systems take place (Sim, 2016).

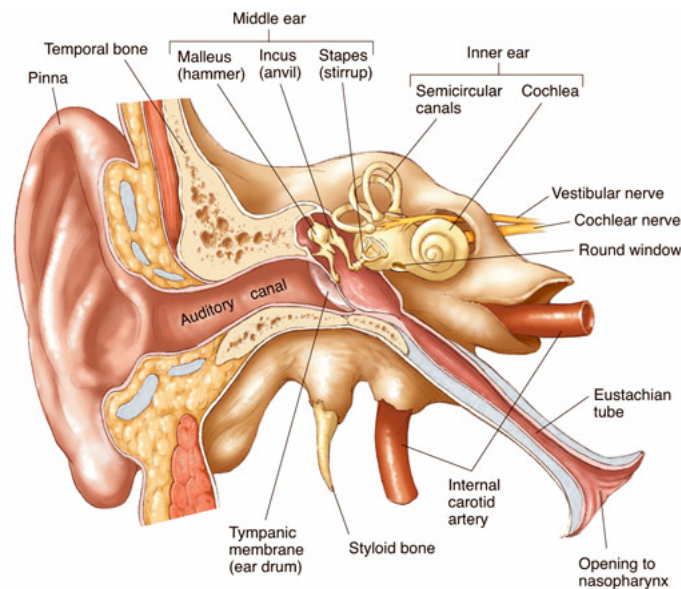


Figure 1 - Diagram of the Ear, (Ear Anatomy, 2006)

Sim further explained that the human cochlea is a spiral shape, making 2.5 turns. The cochlear structures include three ducts, namely the scala vestibuli in the superior, scala tympani in the inferior, and scala media (also called cochlear duct) between them. In the basal end, the scala vestibuli interacts with the stapes footplate via the oval window, and the scala tympani terminates at the round window. The scala media and scala tympani are separated by the cochlea partition,

which consists of the basilar membrane and lateral support structures. The partition that separates the scala vestibuli from the scala media, which is called the Reissner's membrane, provides electrical and chemical insulation, and has a negligible stiffness from a viewpoint of mechanics. The organ of Corti, which sits on the top of the basilar membrane and is embedded in the scala media, is responsible for transducing mechanical motion of the basilar membrane to electrochemical signals. The spiral ganglion provides pathways of the electrochemical signals to the auditory nerve (Sim, 2016).

Middle and Inner Ear Research

Extent of Current Research

Due to the complexity of the human ear there are many different variables that must be explored in order to get a comprehensive understanding of the processes that take place allowing humans to hear. Nakajima et al. explain that most of the research surrounding human ears has been focused specifically on the middle ear. The stapes velocity has been one of the main focuses of research for many, providing useful information regarding sound transmission by air conduction. Although research

has provided us with a better understanding of the middle ear we still lack knowledge about the inner ear, and the conductive pathologies remain an unfamiliar territory. Recent research has attempted to fill this void of information by performing differential pressure measurements at the cochlea base, specifically focusing on the difference between the scala tympani pressure (P_{ST}) and scala vestibuli pressure (P_{SV}), these two channels within the cochlea are shown in Figure 2. The vibration of the stapes produces pressure within the scala vestibuli resulting in motion of the cochlear fluid; the sound pressure is then relieved by the round window in the scala tympani resulting in a pressure difference across the partition that separates the scali. This differential pressure ($P_{SV} - P_{ST}$) is the input signal to the cochlea and ultimately drives the auditory transduction (Nakajima, 2009).

According to Nakajima et al. researching this differential pressure can provide insight into various middle and inner ear pathologies and modifications, such as ossicular discontinuity and semicircular canal dehiscence. It could also provide useful information on stimulating the cochlea in an unconventional method. Ultimately, these measurements will provide a baseline for comparison with future measurements to answer clinically relevant questions (Nakajima, 2009).

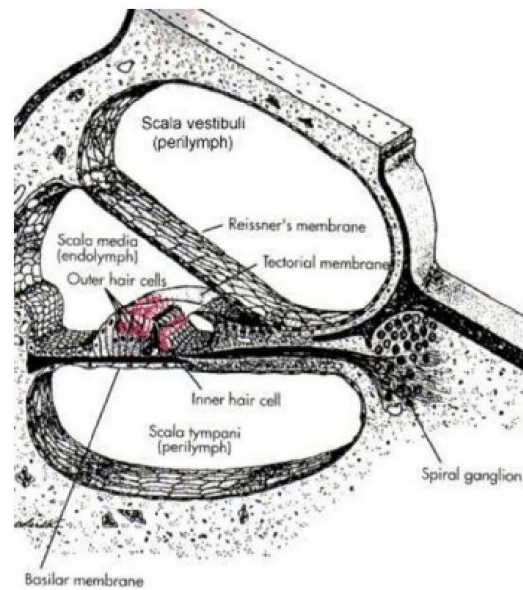


Figure 2 - Cross Section View of Cochlea (Sim, 2016)

Research at the UniversitätsSpital Zürich (USZ)

Currently a research team at UniversitätsSpital Zürich (USZ) is investigating this differential pressure distribution within the inner ear, specifically ($P_{SV} - P_{ST}$) within the cochlea. They require a method of accessing the scala tympani and scala vestibuli of the cochlea by drilling the surrounding temporal bone and inserting a MEMS-based hydrophone (Pffiffner et al., 2016). The location the hydrophones are placed within the inner ear during these experiments is shown in Figure 3.

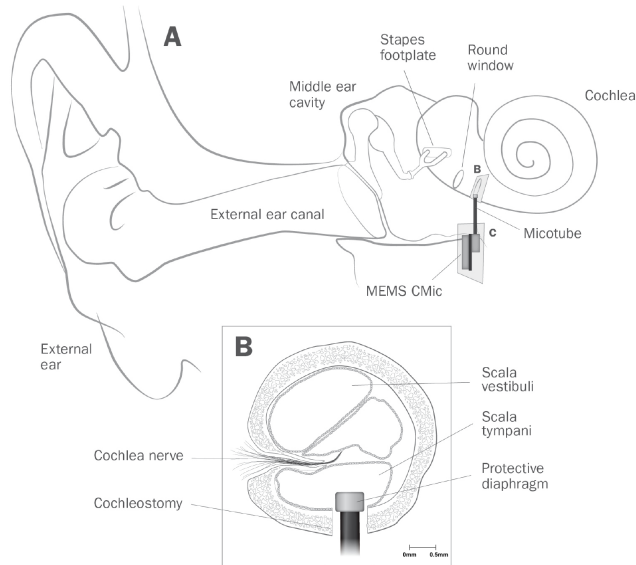


Figure 3 - Representation of ear anatomy with the hydrophone inserted into the cochlea (Pffiffner et al., 2016)

The drilling operation through the temporal bone, as well as the resulting access channel trajectory and diameter, need to be controlled within an accuracy of 1000 microns (1mm). The drilling operation into the cochlea and the insertion of the hydrophone need to be controlled within 250 micron accuracy. An overview of the current drilling procedure applied by the USZ team can be seen in Appendix A. Currently this process is based solely on the experience of an otology surgeon. The hydrophone insertion procedure relies on a custom micromanipulator that is controlled manually by the researchers based on visual feedback from microscopes and cameras. In order to define the location of the hydrophone, the USZ team registers the location of the micromanipulator tool relative to the temporal bone sample. The physical registration procedure involves a metal stylus with a sharp point, which is used to contact or physically touch multiple (i.e. 4-6) fiducial markers rigidly attached to the sample. These markers are metal wires that are 50 microns in diameter solidly embedded within a silica tube for structural support. After this registration the metal stylus is carefully switched with the hydrophone, which is inserted into the sample to obtain pressure measurements. Swapping the tool during this step significantly decreases the accuracy of the hydrophone positioning because these two tool tips are not at the same position relative to the manipulator wrist. The sample is then volumetrically scanned with a commercial μ CT40 scanner manufactured by Scanco Medical in Switzerland (5-15 micro voxel size, $1-10 \times 10^9$

voxels), and the location of the hydrophone is determined post insertion. This location is first estimated based on the location of the end of the cochleostomy and the insertion depth, and is checked by comparing the μ CT scan data and micromanipulator coordinates to each other. This means that in this procedure it is not known until after the experiment whether or not the hydrophone was correctly positioned. This research team has expressed great interest in a future experiment that would consist of placing several of these hydrophones along the lengths of each scala in order to obtain data regarding the entire pressure distribution within the cochlea. However, because they do not currently have the means to efficiently and accurately place these hydrophones this has not been a feasible experiment for them. A representation of a future pressure experiment with multiple hydrophones inserted into the cochlea to explore the pressure along the entire length of the scala tympani and scala vesibuli is shown in Figure 4.

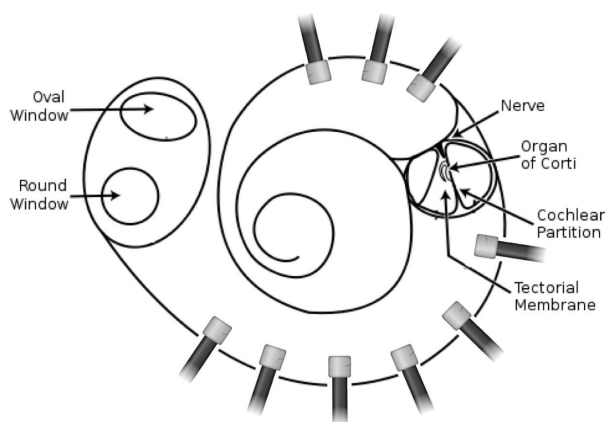


Figure 4 - Representation of future pressure experiments with multiple hydrophone insertions

The miniaturized MEMS based hydrophone that the USZ team is in the process of developing has gone through several different design iterations. Development of the third version of the prototype is currently underway. Figures 5 and 6 contain images of the second version of the hydrophone that is currently being used for pressure distribution research.

These hydrophones have very delicate membranes on the tip of them and can easily be destroyed if they come into physical contact with anything. For this reason the hydrophone itself cannot be used in the physical registration process of the temporal bone sample and must be put into the manipulator only after the physical registration has been done using a metal stylus to come in contact with the fiducial marker. These hydrophones function by the sound induced pressure variations in the cochlea inducing motion of the diaphragms of the sound receiving element, which in turn cause

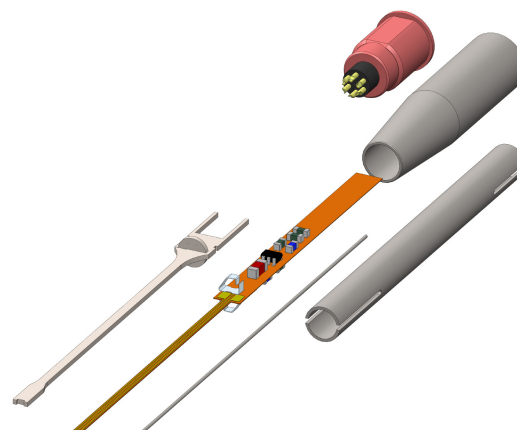


Figure 5 - CAD Model of Hydrophone (Pffifner et al., 2016)

pressure variations within the inert gas of the micro tube that are registered by the MEMS transducer. Based on commercially available MEMS condenser microphones, prototype sensors have been customized for sound measurement in a fluid environment (Elizabeth et al., 2015).

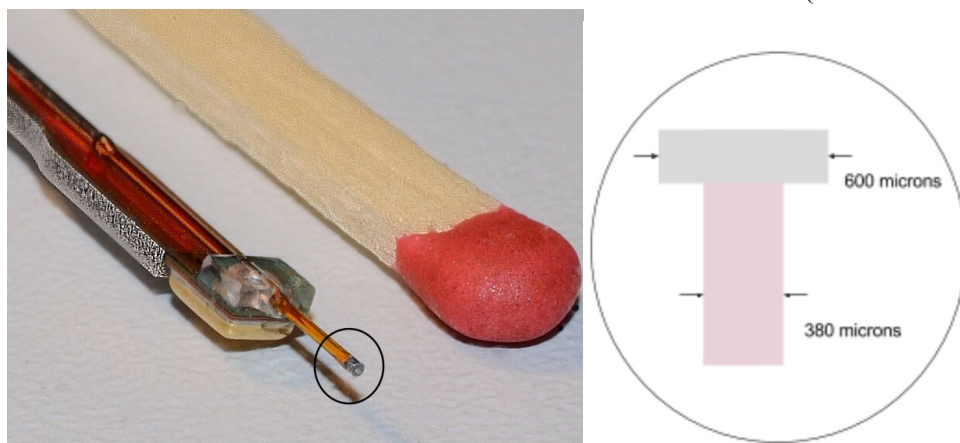


Figure 6 - Close up of Hydrophone Tip (Left) Hydrophone Tip Dimensions (Right)

Minimally Invasive Surgical Techniques

Due to the scale of the human ear, minimally invasive surgical techniques must be utilized when performing procedures such as the hydrophone insertion into the cochlea. One of the most common minimally invasive techniques, used primarily in neurosurgery, is stereotactic surgery. Stereotactic techniques are used for small scale surgeries where accuracy and precision are crucial. These techniques rely on a three-dimensional coordinate system and a physical frame of reference for locating small targets within the body. During these procedures a mechanical device is often used to ensure that the patient's head remains in a fixed position relative to the coordinate system, allowing the surgeons to reach their target location with minimal uncertainty (Levy, n.d.). Computer assisted surgery (CAS) has also been becoming more prominent within minimally invasive surgeries (Nguyen et al., 2011). CAS allows the surgeons to virtually plan the surgery using scan data and then use the information as a guide during the procedure as well.

A research group at Vanderbilt University Medical Center has developed micro-stereotactic techniques to achieve desired approach angles for cochlear access. The resolution of their systems remain greater than 1000 microns (Labadie et al., 2010). Another group in France has been working on a semi-automated robot based system to reduce the error of the alignment of the insertion axis (Torres et al., 2017). A third group at the University of Bern has developed an approach using software that allows them direct cochlear access with positioning accuracies of 150 ± 80 microns (Gerber et al., 2014). Although there has been sufficient research and development for systems to access the cochlea, no current research has attempted to achieve these positioning accuracies for navigation within the cochlea itself that are needed for clinical research purposes.

CT Scanning

Many minimally invasive surgical techniques rely on some form of imaging to get a view of interior anatomy in a noninvasive way. This can be accomplished through various forms of scanning, such as the computed tomography (CT) scan. A CT scan makes use of x-rays to create a 3D view of an object through image slices. The basic idea is that there is a source, which emits the x-rays, and a detector, which picks up the x-rays that have different levels of intensity based on how much it was absorbed by the material it passed through. After rotating around the object, the data from the detector goes through a mathematical transformation, such as a Radon transform, to reconstruct a slice, or several slices, from multiple projections to get a full view of the object (Wang & Vannier, 1999; Weisstein, 2017). These slices can then be put together with an image processing software to get a full 3D view of the object.

A typical CT scan can provide a resolution on the scale of about 1 mm (UTCT, 2016). In the case of the middle and inner ear, it is necessary to have a higher resolution view, as the structures are a much smaller size than other body parts. For this, and similar applications, there is the μ CT scanner. This works in the same way as a regular CT scan, but with a resolution of about 10 microns, and gives clearer results of the bony structures than an MRI would of the same sample (Sim, 2007).

Errors Within Image Registration Systems

Although there are several different types of surgical registrations systems in use today, the majority of them rely on some form of image registration where different sets of data must be transformed into one common coordinate system (Mezger, Jendrewski, & Bartels, 2013). The three main types of error common to image registration are fiducial localization error (FLE), fiducial registration error (FRE), and target registration error (TRE).

Fiducial localization error is defined as the distance between the actual marker locations and the selected marker locations during registration. FLE describes the error that stems from selecting the fiducial markers because the exact location of the markers is unknown. This error value is estimated by averaging the measured distances between repeated selections of the same marker. The fiducial registration error describes the error in alignment between the image space and the physical space that are being aligned. This is calculated using the root mean square distance between corresponding fiducial markers after the registration has taken place. Surgeons often interpret the FRE as an indication of a system's accuracy and ability to provide guidance during surgical procedures. The final type of image registration error, TRE, evaluates the distance between a target location in the physical space and the image space after registration. The difference between FRE and TRE is that TRE involves a target other than the fiducial markers (Datteri & Dawant, 2012; Shamir, Joskowicz, Spektor, & Shoshan, 2009).

Chapter 3: Objectives

The main objective for this project was to improve a current experimentation procedure used by the research team at USZ for inner cochlear acoustic research. Specifically the improved procedure needs to achieve tool positioning on temporal bone samples with accuracies that are below 250 microns. The three tools primarily used in these experiments: the metal stylus, otology drill, and hydrophone, must all be able to achieve these accuracies and be interchangeable on the micromanipulator used for tool maneuvering during the experiments.

Chapter 4: Methodology

In order to complete this project objective several intermediate tasks had to be completed. The first step was to develop a tool calibration setup and procedure for the tools being used in the experiments. This was necessary in order to make them interchangeable on the manipulator and eliminate the positioning errors that currently derive from this step. This was followed by a physical registration using these tools, and then a series of insertion tests to verify the accuracy of these tools. A virtual registration was also completed separate from the physical ones. This allowed for the registrations from the image space and the physical space to be compared to each other through a point cloud to point cloud registration in order to provide feedback on the precision and accuracy of the overall insertion procedure. Each of these steps are described in further detail throughout this chapter.

An overview of the improved experimentation procedure is seen in Figure 7. The major changes from the previous procedure, that can be seen in Appendix A, occur in the preoperative planning, registration, and final insertion and drilling steps. The preoperative planning was not present in the previous procedure because the USZ team had no means to reach the targets they selected in the image space with the manipulator. The error resulting from changing tools was significant enough to make any preoperative planning attempts irrelevant. Although the physical registration was still present in the previous procedure, the tool calibration setup now allows for the physical registration to take place with a force sensor. This allows for a more consistent and expedited registration process. Finally the greatest benefit of this new procedure is that all the preceding steps allow for the final insertion location of the hydrophone to be known within a certain accuracy. This allows the USZ team to know if they are in the correct location before carrying out the entire experiment and going through a second μ CT scan.

Improved Pressure Experiment Procedure

PRE-OPERATIVE

sample Preparation



1. SURGICAL PREPARATION

- Trimming – Cut down temporal bone sample to correct size for scanner cylinder
- Coarse Drilling – Continue cutting down sample to expose target region

2. TECHNICAL PREPARATION

- Fiducial marker Installation - A minimum of three 50 micron diameter metal wires are put on sample

3. PRE-OPERATIVE PLANNING

- μ CT Scan of Sample
- Process Scan Data – Upload data into AMIRA and isolate markers
- Virtual Planning – Using CAD program define the target location, approach vector, and insertion depth

Experiment on sample

INTRA-OPERATIVE



4. REGISTRATION

- Physically touch fiducial markers with force sensor to obtain coordinates
- Using MatLab perform point to point cloud registration to align manipulator and scan data coordinate systems

5. FINAL DRILLING AND INSERTION

GUIDED DRILLING

Using the calibrated stylus or a calibrated laser as a guide to the target location, the drilling can manually be performed with the otology drill.

HYDROPHONE POSITIONING

With a calibrated hydrophone, insertion into the opening in cochlea will take place with a **known** final target location based on the preoperative planning.

Figure 7 - Overview of Improved Pressure Experiment Procedure

Tool Calibration

The first step in improving the procedure used by the researchers at USZ was to calibrate the tools that are used in their pressure measurement experiments. These tools are a metal stylus, a force sensor, and a hydrophone pressure sensor.

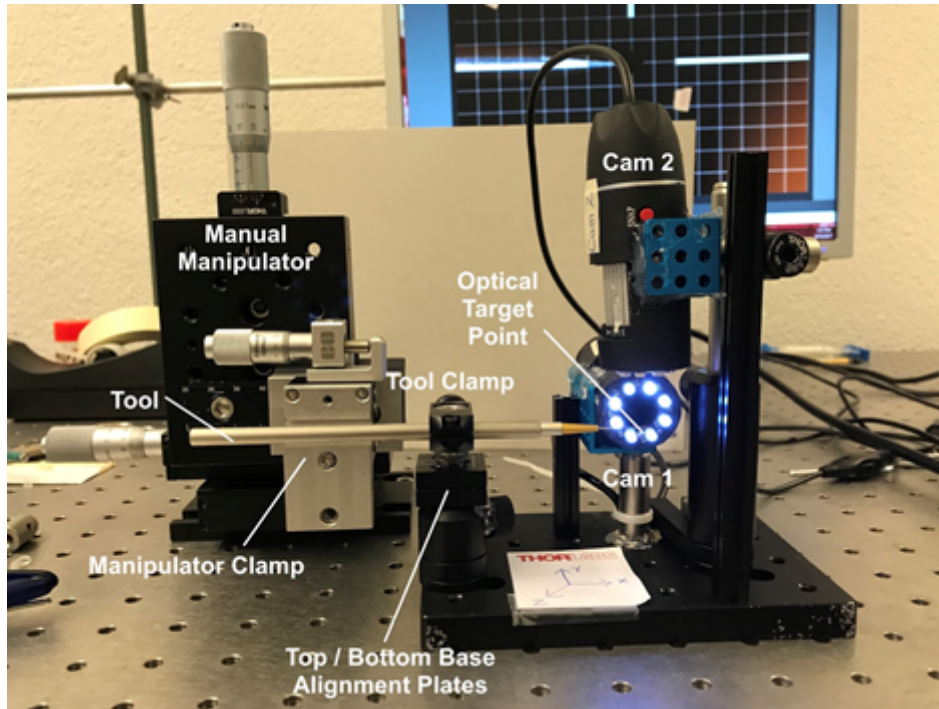


Figure 8 - Tool Calibration Setup

To achieve the goal of calibrating all the tools to the same point, we constructed and used an optical setup as shown above in Figure 8. This consisted of two high resolution cameras (Camera 1: 1600x1200px, Camera 2: 640x480px) aligned at approximately 90 degrees to each other to get a side and top view of the tool. The tool was brought into the field of view of the cameras using a 3 stage manual manipulator that was attached to the tool with the manipulator clamp. Each tool was aligned to the same virtual target point in the cameras and permanently fixated in this position with the tool clamp. This ensured that all tools were calibrated to the same point relative to the base alignment plate, which are kinematic plates that use magnets and allow for a strong yet detachable connection to the calibration setup and the manual manipulator used in the experimental setup. For the purpose of testing the overall procedure there was an additional manipulator stage to allow for installation of the hydrophone tips that were left as markers in the temporal bone sample.

In order to use the cameras as measurement tools and see how accurately we were able to

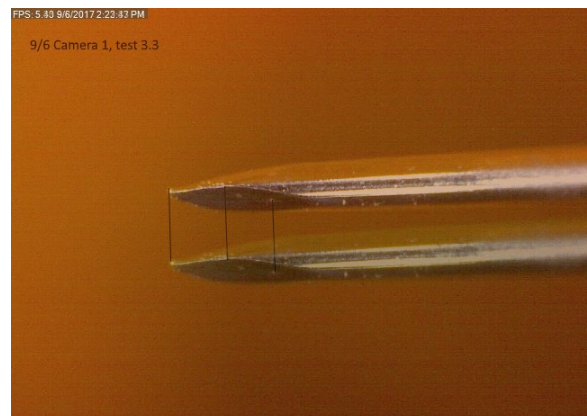


Figure 9 - Overlay Showing Tool Movement with Measurement Lines

achieve alignment to the optical target, it was necessary to determine the scale of the cameras in terms of microns per pixels. This was done by taking an initial picture of a tool tip in both cameras and then moving it a known amount with the manipulator, in this case 1 mm. We then took another picture of the tool tip. Overlaying these two images we were then able to measure the pixel distance that the tool tip travelled as seen in Figure 9. This provided us with a scale in microns/pixel that we were then able to use to measure how much our tools tips deviated from the target location. For camera 1 this was 9.25 microns/pixel and for camera 2 it was 5.36 microns/pixel. After calibration of our three tools the largest deviation from the target was 30 microns, which will contribute to the fiducial localization error and therefore the overall error in the hydrophone insertions.

Initial Registration

Physically touching each of the fiducial markers is a necessary step in completing the overall registration procedure. This physical registration is used to obtain the coordinates of the fiducial markers in the physical space that will then be utilized in the point to point cloud registration to compare to the image space. In the improved procedure the force sensor is the primary tool responsible for completing this physical registration, however it was also done with the metal stylus in order to compare the accuracy of the previous procedure the researchers at USZ established to that of the improved procedure.

Four separate physical registrations of each of the five fiducial markers were carried out using both the previously calibrated force sensor and metal stylus. The data from these registrations can be seen in Appendix B. The setup used for the physical registration is shown in Figure 9.

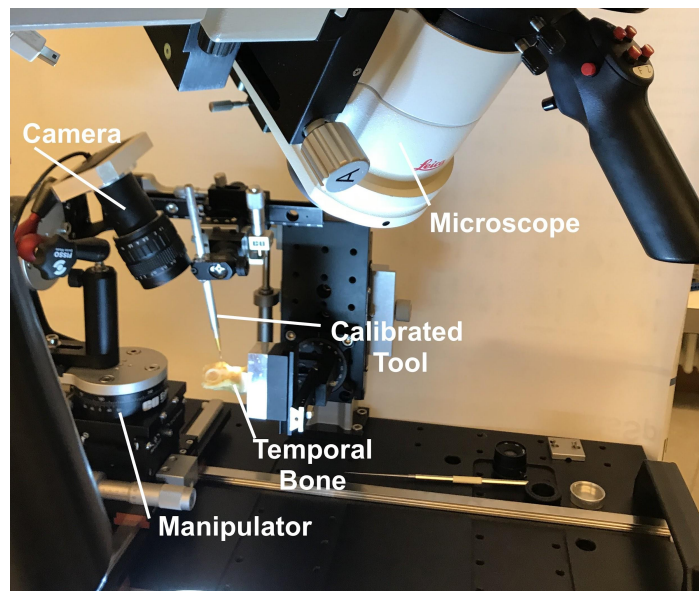


Figure 10 - Physical Registration Setup

The metal stylus required two optical means in order to locate the fiducial marker, one observing the x and y direction allowing for lateral alignment while the other one observed the z direction

providing feedback on the vertical position. This setup was slightly modified when using the force sensor as a second optical tool was no longer needed. Instead, the Sensoptic program that the force sensor uses provided audible feedback when 1 mN of force was detected at the tip of the sensor, therefore alerting the user that the desired lateral position of the tool relative to the marker had been achieved. This specific force value was chosen because it is the lowest detectable value of this particular force sensor. After locating a fiducial marker the x, y, and z locations were then read on the dials of the manipulator stages and recorded to be used later in the point to point cloud registration. This process was then repeated for the four other fiducial markers to complete an entire physical registration. The coordinates recorded from these registrations are limited to the resolution of the manual manipulator used, which is 10 microns.

Virtual Registration

During the virtual registration the same procedure was carried out as in the physical registration. This time, however, it took place on the computer model of the temporal bone that was generated from the CT scan data. Using several thresholding tools within AMIRA the metal markers were isolated from the bone and tissue in the sample. Once the markers were isolated it was possible to place a point on the fiducial marker tips and obtain the (x,y,z) coordinates of each one of the markers. This can be done in various CAD or imaging softwares once the markers have been isolated from the sample. For these experiments the virtual registration took place in Geomagic and the preoperative planning took place in Geomagic as well. Just as for the physical registration, the virtual registration was completed four times to obtain sufficient data. Figure 10 shows the virtual reconstruction of the temporal bone sample in AMIRA.

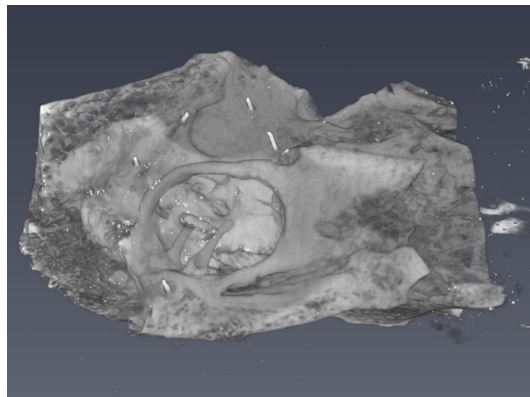


Figure 11 - Virtual Reconstruction of Temporal Bone Sample

Point to Point Cloud Registration

Using the data from our physical and virtual registrations, as described in the sections above, we then aligned our coordinate systems to each other. This was done by finding the optimal rotation and translation between the sets of points. To do this we solved for R and t in the equation below.

$$B = R \cdot A + t$$

To find the optimal transformation matrix we found the centroid of each dataset, which is calculated using the following equations.

$$P = \begin{bmatrix} x \\ y \\ z \end{bmatrix}$$

$$centroid_A = \frac{1}{N} \sum_{i=1}^N P_A^i$$

$$centroid_B = \frac{1}{N} \sum_{i=1}^N P_B^i$$

After finding the centroids, we then needed to find the optimal rotation between points. The most common way of doing this is through singular value decomposition which can be done using Matlab with the formula below (Ho, 2013; Besl & McKay, 1992).

$$H = \sum_{i=1}^N (P_A^i - centroid_A)(P_B^i - centroid_B)^T$$

$$[U, S, V] = SVD(H)$$

$$R = VU^T$$

By using these equations in Matlab we were able to optimize between trials and between markers to find the best alignment of the coordinate system defined in AMIRA and the one defined by the micromanipulator.

Final Procedure Test

To test the accuracy of the improved procedure we conducted several insertion and drilling tests. These tests were broken down into two main groups we defined by angle 1 and angle 2. We aimed to do insertions into various locations to simulate a wide range of experiments that could be using this improved procedure. At angle 1 insertions took place into a pre existing cochleostomy in the scala tympani, round window, an arbitrary location, and finally into the cochlea after performing a cochleostomy. This cochleostomy was performed by carrying out the preoperative planning in a CAD software called Geomagic and then using the manual manipulator with the metal stylus as a guide for the manual drilling process. At angle 2 insertions took place into the scala vestibuli and a second arbitrary location on the sample. These two angles provided data from 6 total insertions.

For each angle a physical registration and a virtual registration had to take place as previously described, the data from these registrations can be seen in Appendix C. These physical registrations were then used in the point to point cloud registrations and we were able to then carry out preoperative plans to determine our insertion locations and dial them in with the manual manipulator. The data for both of the point to point cloud registrations can be seen in Appendix D, this also includes the optimization parameters to determine what fiducial markers to use in the registration that provide the best alignment of the two coordinate systems. At this point the tool was switched to the hydrophone, which was set up with dummy markers attached instead of the functioning sensor. We moved the hydrophone to location determined in the pre operative planning and using glue we left the marker attached to the sample. The locations determined in the preoperative planning can be seen in Appendix E. After all 6 insertions were completed another μ CT scan was conducted to determine the accuracy of the insertions. This scan was again uploaded into AMIRA and then a .STL file was exported to Geomagic in order to extract the locations of the hydrophones. An image of the surface constructed from this post operative scan with the hydrophones inserted can be seen in Figure 11. The green represents the temporal bone itself while the hydrophone tips can be seen in purple. The physical and virtual registration data can also be seen in this image. The black circles labelled with “MP” represent the coordinates of the registration for a fiducial marker using the manipulator while the red stars labelled “CT” represent coordinates of the registration for a fiducial marker using the virtual model. This visual representation allows us to see if there are any major errors within the registration that could be disrupting our experiment, i.e. if the corresponding black circles and red stars do not line up with each other.

This test was used to simulate the practical application of our project, in which the researchers use the calibrated tools and virtual registration to decide where to insert the hydrophone to obtain pressure measurements. It also tested the accuracy of our procedure in checking the ground truth location from the μ CT scan (visualized with AMIRA) to the physical location of our tool. This experiment also provided us information about the error that comes from switching between tools.

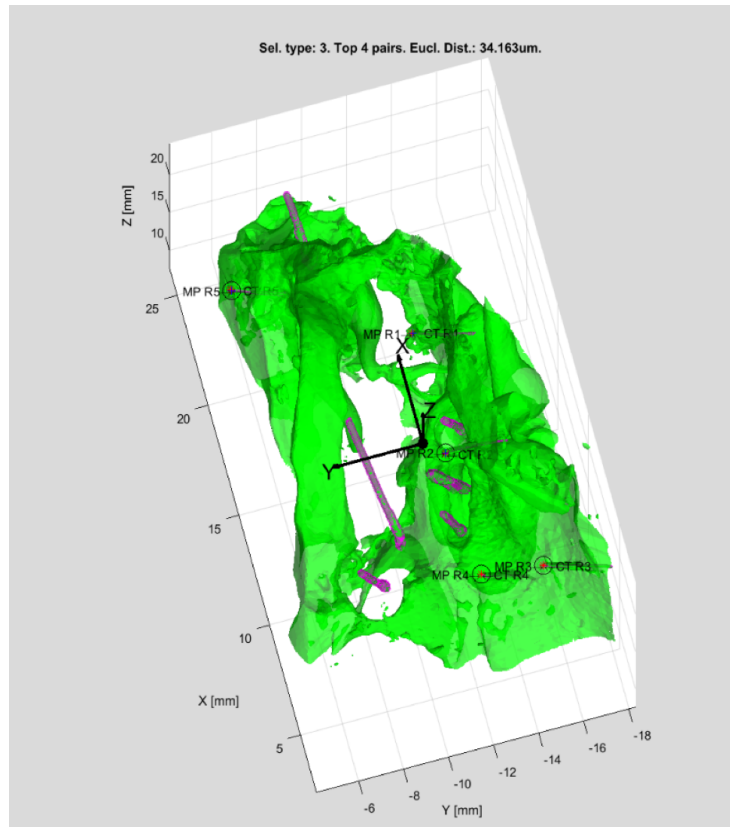


Figure 12 - Post Operative CT Scan Reconstruction

Chapter 5: Experimentation and Results

Initial Registration

Fiducial Localization Error

Figures 12, 13, and 4 display the fiducial localization error, or the error associated with the repeatability of choosing the fiducial marker locations, for the three different tools we used during selecting points. The imaging software consistently had a lower FLE than the physical tools. The metal stylus had a significantly higher error than the force sensor due to its reliance on the camera views to know when a marker is touched. This shows the error in the x, y, and z components, as well as the Euclidean distance for each. Using the force sensor in our improved procedure brings the FLE down from 345 microns with the metal stylus to 39 with the force sensor. This significant decrease in FLE will have a great impact on reducing the overall TRE as well. Along with reducing the error, using the force sensor enables the researchers to quickly carry out the physical registrations because it is now easier to identify when physical contact is made. With the metal stylus registrations took approximately one hour to register 5 fiducial markers and with the force sensor this took about twenty minutes.

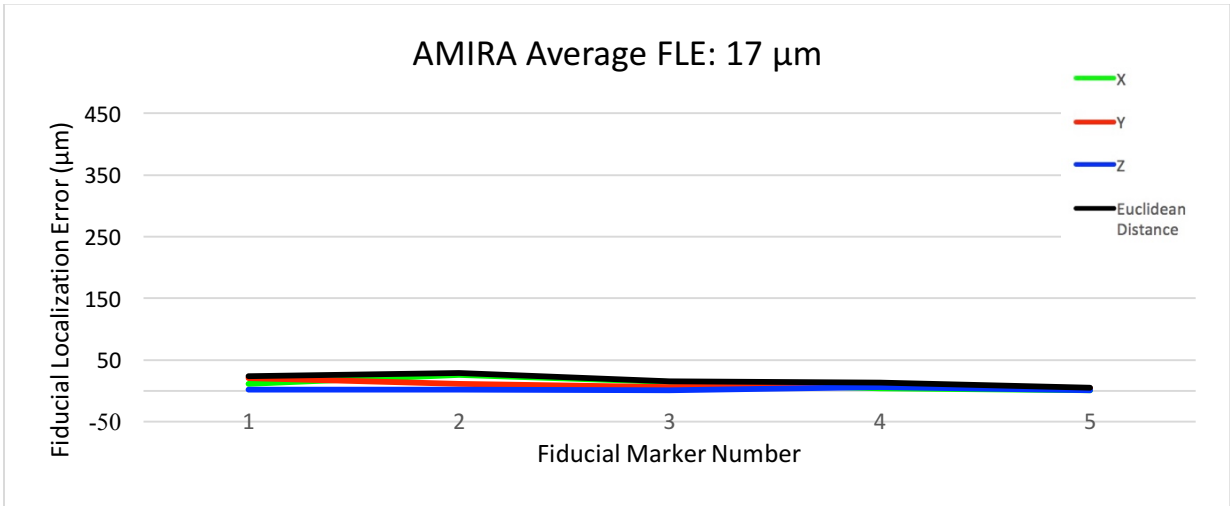


Figure 13 - FLE for AMIRA

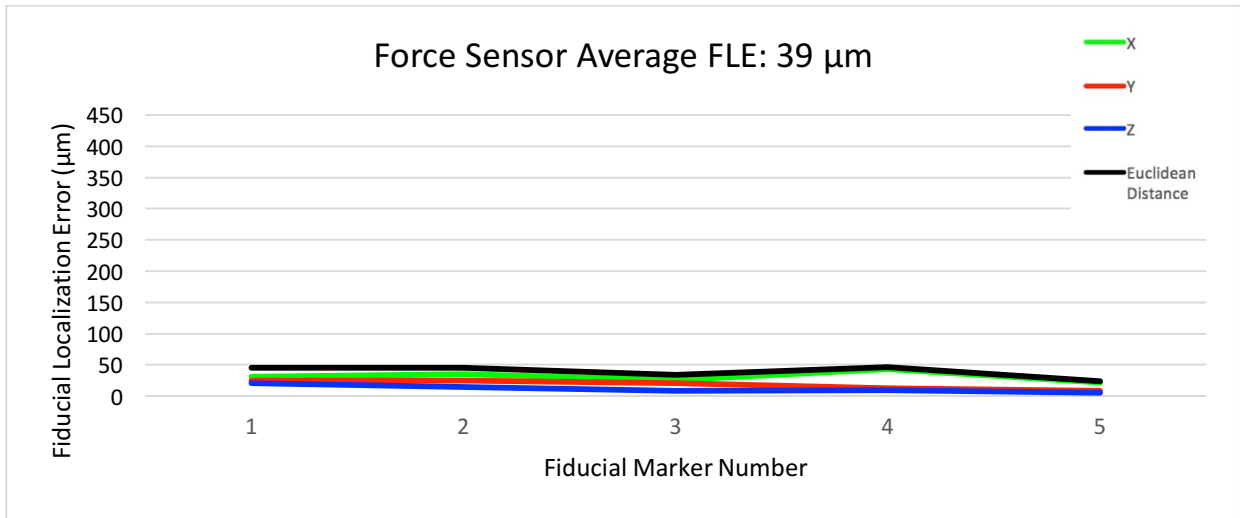


Figure 14 - FLE for the Force Sensor

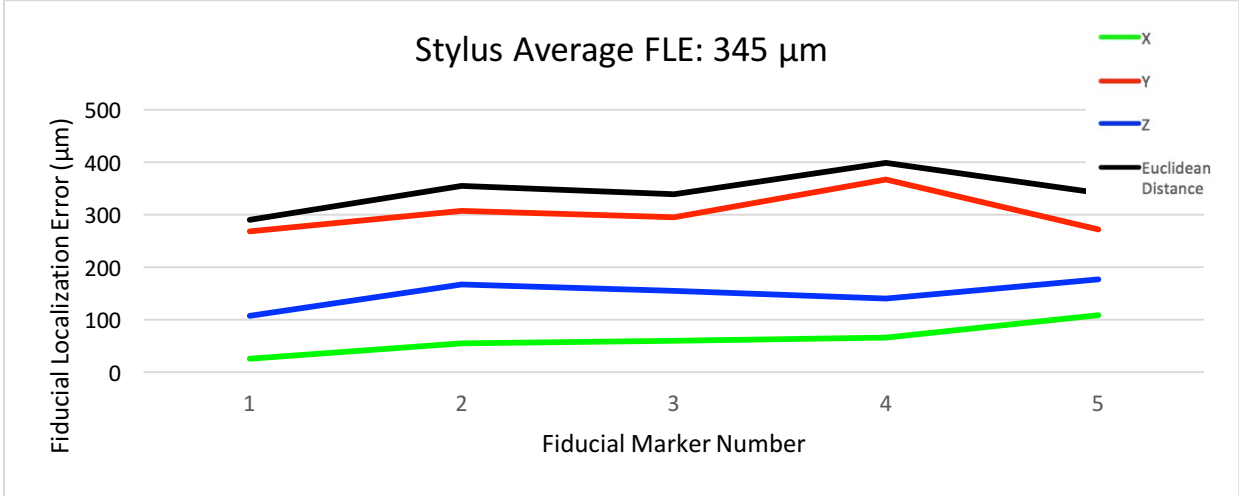


Figure 15 - FLE for the Metal Stylus

Final Procedure

Fiducial Registration Error Using Force Sensor

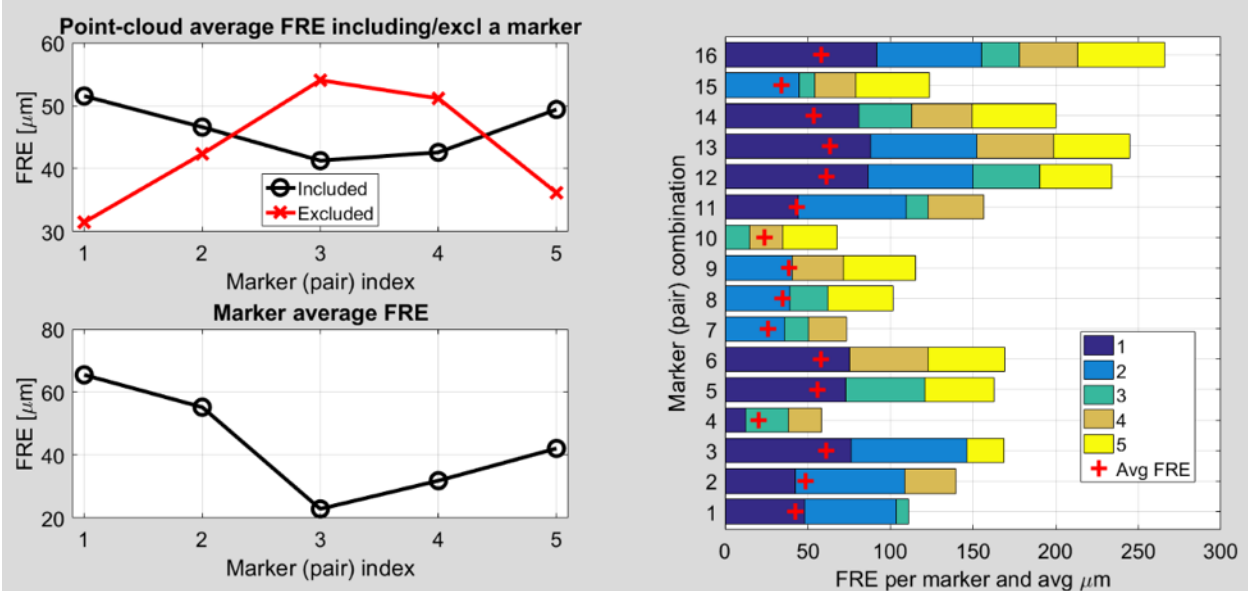


Figure 16 - Overview of all FRE per combination, per marker and per point-cloud average for Angle 1

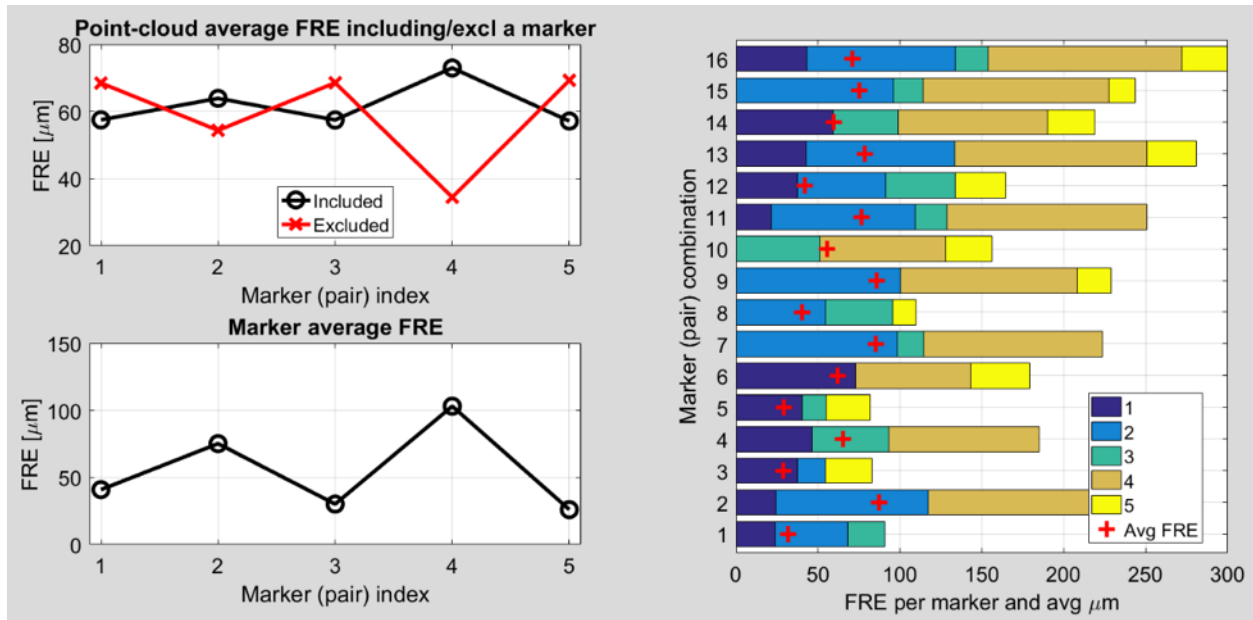


Figure 17 - Overview of all FRE per combination, per marker and per point-cloud average for Angle 2

These graphs show several different representations of the Fiducial Registration Error from the two angles that we used for the final insertion procedure. The graph in the top left shows the average point-cloud FRE, where the black line shows the average when that specific marker is included, and the red line shows the average when that marker is excluded. A significant difference between the red and black lines, when the red is lower, indicates that that marker is likely contributing a large amount of error to the overall registration. If there is a significant difference and the red is higher, meaning the FRE went up when that marker was excluded, this means that that specific marker probably contributed little error to the registration. The graph in the bottom left shows the average FRE for each marker, the distribution of which can be visualized by the different blocks of color in the graph to the right. This graph shows the different combinations of markers that can be used in registration and the FRE that comes from each one. This shows how the markers can contribute to error differently depending on the combination. There is also a crossmark that shows what the average FRE is for each combination. The results from angle 1 shown in Figure 15 are associated with a FRE of about 35 microns. The results from angle 2 shown in Figure 16 are associated with a FRE of about 40 microns. These FRE's contribute to the overall TRE that we had during these insertions.

Target Registration Error Based on Six Hydrophone Insertions at two Angles

The table below shows the target registration error for the six separate insertions from our final procedure. This target registration error provides us feedback on the overall accuracy of our improved insertion procedure. These values represent how closely we were able to physically achieve the target location that we picked on the virtual model. Its worth noting that the highest errors seemed to occur in the axis that is along the length of each of the hydrophones. This error could potentially come from the metal paint coating that was applied on the tip of the hydrophones

so they would show up in the CT scan. This added thickness from the layer of paint could be the reason for this coordinate generally having a larger error than the others. Overall, the average target registration error is below 200 microns. The root mean square for angle 1 is 180 microns and for angle 2 it is 160 microns, these values confirm that we achieved the overall objective for this project of 250 microns.

Table 1 - Target Registration Error for Six Insertions

Insertion Location		Diff in Mech coord			
		X (μm)	Y (μm)	Z (μm)	Euclid. (μm)
Angle 1 (view 1)	Scala Tympani	21	-76	123	146
	Round Window	42	-65	193	208
	Cochleostomy	-188	90	31	211
	Arbitrary 1	12	-124	10	125
Angle 2 (view 2)	Scala Vestibuli	166	69	-35	183
	Arbitrary 2	-116	-48	-56	138

Chapter 6: Discussion

Within this work we proposed an improved experimental procedure for inner cochlear acoustic research. More specifically this procedure was to achieve tool positioning accuracies on the samples of interest within 250 microns. The results of our tests provide a target registration error that confirms we were able to achieve an accuracy below 200 microns when positioning a hydrophone into the temporal bone sample.

Compared to previous experiments, our research goes beyond solely accessing the cochlea as other groups have studied. In the experiment performed by Torres et al. the semi-automated robot based system that was developed was meant to assist the surgeon in a typical cochlear implant procedure, even though it was tested on temporal bone samples as in our experiment (Torres et al., 2017). Our procedure, on the other hand, allows for researchers to access the cochlea from different angles to obtain pressure measurements along the entire structure. The downside to this is that it is not immediately applicable to use on patients, instead being meant for research purposes alone. In the experiment done by Labadie et al. a similar stereotactic method was used on patients, but did not have the level of accuracy that was achieved in our procedure (Labadie et al., 2010). The group at the University of Bern achieved comparable results to our experiment, and as both used similar approaches this is to be expected. Their focus was on surgical planning for direct cochlear access and testing software to choose the insertion axis, whereas our focus was on the physical positioning and insertion of the hydrophone (Gerber et al., 2014).

This improved procedure provides additional benefits for carrying out inner cochlear acoustic experiments. Due to the preoperative planning that takes place virtually on the scanned sample, the time the sample is exposed to the environment during the experiment is now

minimized. This will provide more accurate experiment results as the samples begin to change on a molecular level as they dry and lose certain characteristics as soon as they are exposed to the environment. This procedure also provides the benefit of being able to insert multiple hydrophones efficiently and effectively into the cochlea during a single experiment. This will allow researchers to begin the exploration of the sound pressure distribution along the entire length of the cochlea and not just at the beginning of it.

In addition to the immediate benefits of this improved procedure it could also be easily modified to extend its usefulness. Now that the methods for achieving these positioning accuracies have been established they could be applied elsewhere. Calibrating lasers and using them in the manipulator would allow for optical targets to be projected onto the sample with this same level of accuracy. This could be used as a guide for manual drilling. The otology drill used for performing the cochleostomies in these experiments could also be calibrated with the tool calibration setup and then used in the manual manipulator for a semi-autonomous drilling procedure, which would reduce the time during this step of the experiments. It would also eliminate the need for a surgeon during the actual experiments as the researchers could simply follow the preoperative planning data by moving the manipulator to the correct coordinates. Another application would be to carry out this procedure using a robot instead of a manual manipulator. This would again expedite the process and eliminate several steps in the procedure that currently allow for human error to be made, such as with manually dialing in and reading the coordinates on the manipulator. These future applications would have been pursued further had our time with the USZ research team been longer than two months.

Within our project there are several possible sources of error that could influence our final results. The first comes from our calibration. We conducted extensive tests to check our selection error in determining what we are seeing in each camera, and although the error was minimal, it contributes to our fiducial localization errors. There are also possible sources of error in our registrations, as it is difficult to tell exactly what is the tip of each marker, and in the physical system there is always the possibility that things are moving. An example of this is that we are assuming that the micromanipulator holding our tool is perfectly static, but there could be some slight deformations. For the most part, this error is seen in the fiducial registration error.

Another significant source of error comes from the difficulty of inserting the hydrophone. To make the hydrophone visible in the μ CT scan we had covered the tip of it in a metallic paint. This, however, increased the diameter and made it difficult to judge the depth in Geomagic. There was also the difficulty of securing the hydrophone to the sample. We secured it first with super glue and then with epoxy, however because the tool is so delicate adding this glue may have moved it from the intended position. Despite these sources of error, our target accuracy was still achieved.

Although we achieved the desired level of accuracy this procedure could be further improved through repeating the same experiments that we carried out with minor changes. The first recommendation would be to use the same wire used for the fiducial markers during the insertion tests instead of hydrophone tips. This would allow for the tip locations to be picked more precisely on the post operative scan of the sample after the insertions have taken place. We used

hydrophones for the purpose of making the insertions similar to those that the USZ team will perform however smaller diameter metal wires will provide better results for the purpose of testing the improved procedure.

Conclusion

The inner ear has many complex structures and functions, some of which still remain unexplored. The work we have presented will assist in further investigation into the acoustic sound pressure distribution in the cochlea, specifically in the difference between the scala tympani pressure (P_{ST}) and scala vestibuli pressure (P_{SV}). This research attempts to fill the void of information regarding the inner ear in hopes of better understanding pathologies related to these structures. These measurements ultimately provide a baseline for reference against future measurements that aim to answer clinically relevant questions.

The result of this project was an improved accuracy and precision for hydrophone positioning during pressure experiments done by the team at USZ. Our goal was to achieve an accuracy level of 250 microns, which we exceeded with our final results below 200 microns. This means that our procedure can be used for future applications such as autonomous or semi-autonomous drilling, or sample registration and sensor insertion at multiple locations across the same sample.

References

- Besl, P. J., & McKay, N. D. (1992). A method for registration of 3-D shapes. *IEEE Transactions on pattern analysis and machine intelligence*, 14(2), 239-256.
- Datteri, R. D., & Dawant, B. M. (2012). Estimation and Reduction of Target Registration Error. Retrieved August 25, 2017, from <https://www.ncbi.nlm.nih.gov/pmc/articles/PMC4423533/>
- [Ear Anatomy]. (2006). Retrieved October 12, 2017, from <http://www.biographixmedia.com/human/ear-anatomy.html>
- Elizabeth S. Olson, Hideko H. Nakajima, "A family of fiber-optic based pressure sensors for intracochlear measurements", *Proc. SPIE 9303, Photonic Therapeutics and Diagnostics XI*, 93031O (26 February 2015); <http://dx.doi.org/10.1117/12.2178056>
- Gerber, N., Bell, B., Gavaghan, K., Weisstanner, C., Caversaccio, M., & Weber, S. (2014). Surgical planning tool for robotically assisted hearing aid implantation. *international journal of computer assisted radiology and surgery*, 9(1), 11-20.
- Ho, N. (2013, May 10). Finding Optimal Rotation and Translation Between Corresponding 3D Points. Retrieved October 02, 2017, from http://nghiaho.com/?page_id=671
- Labadie, R. F., Balachandran, R., Mitchell, J., Noble, J. H., Majdani, O., Haynes, D., ... & Fitzpatrick, J. M. (2010). Clinical validation study of percutaneous cochlear access using patient customized micro-stereotactic frames. *Otology & neurotology: official publication of the American Otological Society, American Neurotology Society [and] European Academy of Otology and Neurotology*, 31(1), 94.
- Levy, R. (n.d.). A Short History of Stereotactic Neurosurgery. Retrieved August 25, 2017, from <http://www.neurosurgery.org/cybermuseum/stereotactichall/stereoarticle.html>
- Mezger, U., Jendrewski, C., & Bartels, M. (2013). Navigation in surgery. *Langenbeck's Archives of Surgery*, 398(4), 501–514. <http://doi.org/10.1007/s00423-013-1059-4>
- Nakajima, H. H., Dong, W., Olson, E. S., Merchant, S. N., Ravicz, M. E., & Rosowski, J. J. (2009). Differential intracochlear sound pressure measurements in normal human temporal bones. *Journal of the Association for Research in Otolaryngology*, 10(1), 23.

- Nguyen, Y., Miroir, M., Vellin, J. F., Mazalaigne, S., Bensimon, J. L., Bernardeschi, D., ... & Grayeli, A. B. (2011). Minimally invasive computer-assisted approach for cochlear implantation: a human temporal bone study. *Surgical innovation*, 18(3), 259-267.
- Péus, D., Dobrev, I., Prochazka, L., Thoele, K., Dalbert, A., Boss, A., ... & Huber, A. (2017). Sheep as a large animal ear model: Middle-ear ossicular velocities and intracochlear sound pressure. *Hearing Research*.
- Pfiffner, F., Prochazka, L., Peus, D., Dobrev, I., Dalbert, A., Sim, J. H., . . . Huber, A. M. (2016, Dec 16). A MEMS Condenser Microphone-Based Intracochlear Acoustic Receiver. Retrieved August 25, 2017, from <https://www.ncbi.nlm.nih.gov/pubmed/28029613>
- Shamir, R. R., Joskowicz, L., Spektor, S., & Shoshan, Y. (2009). Localization and registration accuracy in image guided neurosurgery: a clinical study. *International journal of computer assisted radiology and surgery*, 4(1), 45-52.
- Sim, J. H. (2007). Imaging, physiology, and biomechanics of the malleus-incus complex (Doctoral dissertation, Stanford University).
- Sim, J. H. (2016). *Brief Description of Human Ear Anatomy* (pp. 1-5, Working paper).
- Torres, R., Kazmitcheff, G., De Seta, D., Ferrary, E., Sterkers, O., & Nguyen, Y. (2017). Improvement of the insertion axis for cochlear implantation with a robot-based system. *European Archives of Oto-Rhino-Laryngology*, 274(2), 715-721.
- UTCT. (2016). Resolution and size limitations. Retrieved from <http://www.ctlab.geo.utexas.edu/about-ct/resolution-and-size-limitations/>
- Wang, G., & Vannier, M. W. (1999). Computerized tomography. *Wiley Encyclopedia of Electrical and Electronics Engineering*.
- Weisstein, E. W. (2017). Radon Transform. From MathWorld--A Wolfram Web Resource. Retrieved October 7, 2017, from <http://mathworld.wolfram.com/RadonTransform.html>
- Zhi, D. (2015). Towards estimating fiducial localization error of point-based registration in image-guided neurosurgery. Retrieved August 25, 2017, from <https://www.ncbi.nlm.nih.gov/pubmed/26406096>

Appendix A: Current Pressure Experiment Procedure

Current Pressure Experiment Procedure

PRE-OPERATIVE

sample preparation



1. SURGICAL PREPARATION

- Trimming – Cut down temporal bone sample to correct size for scanner cylinder
- Coarse Drilling – Continue cutting down sample to expose target region
- Fine Drilling – Carefully expose target location on cochlea
- Define cochleostomy location with superficial drilling on cochlea

2. TECHNICAL PREPARATION

- Artificial Ear Canal (AEC) installation to be used in experiments
- Fiducial Marker Installation - Several 0.05mm diameter metal wires solidly embedded within a silica tube

INTRA-OPERATIVE

Experiment on sample



3. FINAL DRILLING

- Return to previously determined location (from step 1) and complete cochleostomy

4. HYDROPHONE POSITIONING

- Insert hydrophone into opening in cochlea, estimating the final target location and angle
- Collect pressure measurements

5. HYDROPHONE REGISTRATION

- Leave tip of hydrophone as a marker to confirm location

POST-OP

LOCATION ANALYSIS

6. MICRO CT SCAN

- Scan the sample to compare the actual location to the desired location to determine accuracy

Appendix B: Physical and Virtual Registration Data for Initial Registration

	Marker	Physical (Force Sensor)			Virtual (AMIRA)		
		X	Y	Z	X	Y	Z
Trial 1	1	7.62	10.28	9.12	16.45	10.38	16.55
	2	11.52	7.64	11.72	14.75	7.06	20.43
	3	16.66	3.79	10.21	11.29	7.38	26.01
	4	17.98	7.17	9.46	14.45	8.86	27.16
	5	9.00	20.92	4.95	26.17	16.44	17.33
Trial 2	1	7.58	10.33	9.10	16.42	10.34	16.55
	2	11.52	7.59	11.75	14.72	7.04	20.43
	3	16.67	3.81	10.20	11.26	7.36	26.01
	4	17.90	7.18	9.46	14.45	8.84	27.15
	5	8.98	20.91	4.96	26.18	16.43	17.33
Trial 3	1	7.56	10.28	9.15	16.43	10.34	16.55
	2	11.52	7.59	11.75	14.69	7.04	20.43
	3	16.62	3.78	10.21	11.28	7.37	26.01
	4	17.89	7.17	9.46	14.44	8.84	27.15

	5	8.96	20.90	4.96	26.18	16.43	17.33
Trial 4	1	7.55	10.28	9.13	16.43	10.34	16.55
	2	11.45	7.59	11.74	14.75	7.04	20.43
	3	16.62	3.76	10.22	11.26	7.36	26.01
	4	17.89	7.15	9.48	14.44	8.84	27.15
	5	9.01	20.91	4.96	26.17	16.43	17.33

Appendix C: Physical and Virtual Registration Data for Final Procedure

Virtual and Physical Registration Data for Angle 1							
	Marker	Physical (Force Sensor)			Virtual (AMIRA)		
		X	Y	Z	X	Y	Z
Angle 1	1 (REF)	15.8	12.08	23.07	16.45	10.38	16.55
	2	10.39	12.05	23.01	14.75	7.06	20.43
	3	5.49	15.07	19.92	11.29	7.38	26.01
	4	6.61	12.61	17.46	14.45	8.86	27.16
	5	22.00	5.74	15.69	26.17	16.44	17.33

Virtual and Physical Registration Data for Angle 2							
	Marker	Physical (Force Sensor)			Virtual (AMIRA)		
		X	Y	Z	X	Y	Z
Angle 2	1 (REF)	14.65	20.50	24.39	16.45	10.38	16.55
	2	9.31	19.51	23.79	14.75	7.06	20.43
	3	4.51	21.13	19.64	11.29	7.38	26.01
	4	6.27	18.58	17.68	14.45	8.86	27.16
	5	22.79	14.44	18.96	26.17	16.44	17.33

Appendix D: Point to Point Cloud Registration Parameters

ANGLE 1

Fiducial marker position in CT Coord system

```
CT_pos = [14.324999 21.194998 38.837990
          16.049999 24.359999 43.010315
          19.679998 23.789999 48.3532871
          16.529999 22.244999 49.328827
          4.980000 14.610000 39.468342];
```

Fiducial marker position in Mech. Coord system

```
Mech_pos = [5.8 12.08 23.07
            10.39 12.05 23.01
            5.49 15.07 19.92
            6.61 12.61 17.46
            22.00 5.74 15.69];
```

```
Mech_pos(:,2) = -Mech_pos(:,2);%flip Y axis on Mech for RH coord sys
```

Fiducial marker selection optimization:

```
10 combinations for a set of 3
Comb #1(1): 1 2 3
RMSE: 0.042558mm
Reflection detected
Comb #2(2): 1 2 4
RMSE: 0.048731mm
Reflection detected
Comb #3(3): 1 2 5
RMSE: 0.061203mm
Reflection detected
Comb #4(4): 1 3 4
RMSE: 0.020279mm
Reflection detected
Comb #5(5): 1 3 5
RMSE: 0.055918mm
Reflection detected
Comb #6(6): 1 4 5
RMSE: 0.058057mm
Comb #7(7): 2 3 4
RMSE: 0.025986mm
Comb #8(8): 2 3 5
RMSE: 0.034782mm
Reflection detected
Comb #9(9): 2 4 5
RMSE: 0.038738mm
Comb #10(10): 3 4 5
RMSE: 0.023879mm
Elapsed time is 0.015923 seconds.
Elapsed time is 0.003551 seconds.
```

```

5 combinations for a set of 4
Comb #1(11): 1 2 3 4
RMSE: 0.043434mm
Comb #2(12): 1 2 3 5
RMSE: 0.06137mm
Comb #3(13): 1 2 4 5
RMSE: 0.063528mm
Comb #4(14): 1 3 4 5
RMSE: 0.053636mm
Comb #5(15): 2 3 4 5
RMSE: 0.034163mm
Elapsed time is 0.005050 seconds.
Elapsed time is 0.000536 seconds.
1 combinations for a set of 5
Comb #1(16): 1 2 3 4 5
RMSE: 0.05821mm
Elapsed time is 0.002075 seconds.

```

Final registration parameters – rotation and translation:

```

Rot is:
-0.30957   -0.57061   -0.76064
-0.92595    0.36286    0.10465
 0.21629    0.73671   -0.64068

```

```

Trans is:
 61.938
-10.5416
 29.1253

```

ANGLE 2

Fiducial marker position in CT Coord system

```

CT_pos = [14.324999 21.194998 38.837990
          16.049999 24.359999 43.010315
          19.679998 23.789999 48.3532871
          16.529999 22.244999 49.328827
          4.980000 14.610000 39.468342];

```

Fiducial marker position in Mech. Coord system

```

Mech_pos = [14.65 20.50 24.39
            9.31 19.51 23.79
            4.51 21.13 19.64
            6.27 18.58 17.68
            22.79 14.44 18.96];

```

```

Mech_pos(:,2) = -Mech_pos(:,2);%flip Y axis on Mech for RH coord sys

```

Fiducial marker selection optimization:

Elapsed time is 0.013553 seconds.

10 combinations for a set of 3

Reflection detected

Comb #1(1): 1 2 3

RMSE: 0.031838mm

Reflection detected

Comb #2(2): 1 2 4

RMSE: 0.087328mm

Comb #3(3): 1 2 5

RMSE: 0.028851mm

Reflection detected

Comb #4(4): 1 3 4

RMSE: 0.065298mm

Comb #5(5): 1 3 5

RMSE: 0.029257mm

Comb #6(6): 1 4 5

RMSE: 0.062124mm

Comb #7(7): 2 3 4

RMSE: 0.085364mm

Reflection detected

Comb #8(8): 2 3 5

RMSE: 0.040335mm

Comb #9(9): 2 4 5

RMSE: 0.085884mm

Comb #10(10): 3 4 5

RMSE: 0.055592mm

Elapsed time is 0.074200 seconds.

Elapsed time is 0.000781 seconds.

5 combinations for a set of 4

Comb #1(11): 1 2 3 4

RMSE: 0.076622mm

Comb #2(12): 1 2 3 5

RMSE: 0.041981mm

Comb #3(13): 1 2 4 5

RMSE: 0.078591mm

Comb #4(14): 1 3 4 5

RMSE: 0.059664mm

Comb #5(15): 2 3 4 5

RMSE: 0.075236mm

Elapsed time is 0.008590 seconds.

Elapsed time is 0.000721 seconds.

1 combinations for a set of 5

Comb #1(16): 1 2 3 4 5

RMSE: 0.071063mm

Elapsed time is 0.006482 seconds.

Final registration parameters – rotation and translation:

Rot is:

-0.48306	-0.60563	-0.63235
-0.87515	0.3566	0.32702
0.027441	0.71137	-0.70228

Trans is:

58.9953
-28.2099
36.1755

Appendix E: Preoperative Planning Data for Marker Insertions

Insertion Location		Mod. Mech in CT coord		
		X	Y	Z
Angle 1 (view 1)	Scala Tympani	15.18	18.50	46.83
	Round Window	15.13	16.67	44.99
	Cochleostomy	15.12	19.56	48.67
	Arbitrary 1	11.89	21.03	50.20
Angle 2 (view 2)	Scala Vestibuli	12.55	19.78	48.95
	Arbitrary 2	7.96	10.76	40.07